Cerebral Cortex September 2015;25:3000–3013
doi:10.1093/cercor/bhu095
Advance Access publication May 15, 2014

The Neonatal Connectome During Preterm Brain Development

Martijn P. van den Heuvel[1,3], Karina J. Kersbergen[2], Marcel A. de Reus[1,3], Kristin Keunen[2,3], René S. Kahn[1,3], Floris Groenendaal[2,3], Linda S. de Vries[2,3] and Manon J.N.L. Benders[2,3]

[1]Department of Psychiatry, [2]Department of Neonatology, Wilhelmina Children's Hospital, University Medical Center Utrecht, The Netherlands and [3]Brain Center Rudolf Magnus, The Netherlands

Address correspondence to Dr Martijn van den Heuvel, Brain Center Rudolf Magnus, Department of Psychiatry, University Medical Center Utrecht, Heidelberglaan 100, 3508 GA Utrecht, PO Box 85500, Room: A01.126, The Netherlands. Email: m.p.vandenheuvel@umcutrecht.nl

The human connectome is the result of an elaborate developmental trajectory. Acquiring diffusion-weighted imaging and resting-state fMRI, we studied connectome formation during the preterm phase of macroscopic connectome genesis. In total, 27 neonates were scanned at week 30 and/or week 40 gestational age (GA). Examining the architecture of the neonatal anatomical brain network revealed a clear presence of a small-world modular organization before term birth. Analysis of neonatal functional connectivity (FC) showed the early formation of resting-state networks, suggesting that functional networks are present in the preterm brain, albeit being in an immature state. Moreover, structural and FC patterns of the neonatal brain network showed strong overlap with connectome architecture of the adult brain (85 and 81%, respectively). Analysis of brain development between week 30 and week 40 GA revealed clear developmental effects in neonatal connectome architecture, including a significant increase in white matter microstructure ($P < 0.01$), small-world topology ($P < 0.01$) and interhemispheric FC ($P < 0.01$). Computational analysis further showed that developmental changes involved an increase in integration capacity of the connectivity network as a whole. Taken together, we conclude that hallmark organizational structures of the human connectome are present before term birth and subject to early development.

Keywords: connectome, development, functional connectivity, neonatal, structural connectivity

Introduction

The macroscopic brain comprises a large number of anatomically and functionally distinct regions, linked by a complex web of structural white matter pathways, known as the human connectome (Sporns et al. 2005). Adopting network science as a general mathematical framework to visualize and examine the connectome's complex network structure, recent structural and functional studies have reported several hallmark features of adult connectome organization, including the presence of a small-world modular organization with functionally coupled communities, short communication pathways, and the formation of central connectivity hubs facilitating efficient global communication (Bassett and Bullmore 2006; Hagmann et al. 2008; van den Heuvel and Sporns 2011). During what developmental period these hallmark features arise remains however unknown.

The adult cerebral brain network is the result of a complex developmental trajectory. From the prenatal formation of the first neurons, throughout the first years of life and all the way into late adolescents, the brain undergoes an elaborate developmental trajectory. Its developmental period involves an initial exuberant increase in the number of network parts, being neurons, axons, and dendrites, as well as an elaborate growth and transformation of its large-scale wiring pattern. Studies have suggested that the first "predecessor" neurons appear from neuroepithelial cells as early as around the 5th week after conception (see for a detailed review on the development of the embryonic cortex (Bystron et al. 2008)). During the following period, the vast majority of 10 billion cortical neurons are being formed, migrate to their final position, and start to grow their axonal and dendritic projections from which they connect to other neurons, with a steady, but relative slow growth of synaptic connections (Lagercrantz 1998; Innocenti and Price 2005; Stiles and Jernigan 2010; Kostovic et al. 2014). It is during the last weeks of gestation (week >24) (Huttenlocher and Dabholkar 1997; Bruer 1999) that a period of exuberant synapse growth starts, with a synaptic "big bang" occurring around birth (Lagercrantz 1998), indicating the start of a period of exuberant formation of synaptical connections, with a peak of synaptic connections occurring around year 2 of life (Rakic et al. 1986; Huttenlocher and Dabholkar 1997; Bruer 1999; Petanjek et al. 2011; Lagercrantz 1998; Kostovic et al. 2014). This period around birth thus involves a sudden increase in total physical connections and interactions between neurons of the cerebral cortex, and thus involves an important period in cortical connectome genesis (Collin et al. 2014).

The far majority of these neural interactions and synaptic connections take place between neurons on the microscopic scale, with axonal projections linking neurons by means of intracortical and short-range white matter axonal projections (Schuz and Braitenberg 2002; Markov et al. 2011). However, a relatively small fraction involves long-range connections involved in neural communication processes between distant parts of the brain (Schuz and Braitenberg 2002; Markov et al. 2011). It is the early development of these long-distance cortico-cortical connections, to some extent accessible on the macroscopic scale to noninvasive neuroimaging techniques, that is the primary focus of our study. Structural neuroimaging studies have shown that as early as 2 years, and likely even earlier, the vast majority of these long-range cortico-cortical projections are present (Hagmann et al. 2010; Hwang et al. 2012; Khundrakpam et al. 2012; Yap et al. 2011). In parallel, functional studies examining the functional dynamics and functional interactions between brain regions of the young brain have suggested that most functional networks are present in the infant brain (Fransson et al. 2009; Stevens et al. 2009; Smyser et al. 2011), this with later development of the child and adolescent brain mostly involving the transformation of functional connectivity (FC) from a segregated, clustered structure early in life, to a more global and integrated system

during adult life (Fair et al. 2007, 2009; Dosenbach et al. 2010; Power et al. 2010). These neuroimaging studies have elucidated network changes in the postnatal young and adolescent brain, but important open questions about the development of the brain's macroscopic wiring circuitry still remain, in particular about developmental processes during and after the first phases of connectome genesis.

Here, we aimed to study the macroscale connectivity network of the neonatal brain during week 30 and week 40 of gestational age (GA) in preterm born neonates. Using diffusion-weighted and resting-state fMRI data to provide an estimate of the macroscale connections of the brain, we examined the spatial layout of the structural and FC patterns of the neonatal brain during the early phases of preterm macroscopic connectome development.

Materials and Methods

Participants

Twenty-seven preterm infants born with a GA of around (on average) 27 weeks were scanned between week 30 and week 42 of corrected GA (see Table 1 for demographics). Participants underwent a 35-min scanning session in a 3-Tesla Philips Achieva system (Philips Medical systems, Best, The Netherlands). A scanning session included the acquisition of an anatomical scan (T_1 weighted), a diffusion-weighted imaging (DWI) scan, and/or a resting-state functional MRI scan. All neonates were sedated during imaging (see below). DWI data were acquired of in total 23 neonates; in 21 neonates rs-fMRI was acquired (see Table 1). Of 7 neonates, longitudinal DWI scan (i.e., 1 scan at 30 weeks and 1 scan at 40 weeks) was available. Of 7 neonates, longitudinal resting-state fMRI data were available. Of 21 datasets, both resting-state fMRI and diffusion imaging was available, allowing for an examination of a structure–function relationship.

For the cross-sectional analysis, all datasets were included into one structural dataset to maximize statistical power, as regularly performed in infant imaging studies (Berman et al. 2005; Deipolyi et al. 2005; Adams et al. 2010). All data were acquired as part of standard clinical care. For this study, all scans were evaluated by a team of neonatologists and radiologists with extensive experience in neonatal brain imaging. MRI imaging was acquired as part of standard clinical care to examine for potential gray and white matter damage, graded according to the injury scores of Woodward et al. (2006). Only neonates that scored normal/mild on the Woodward scale were included in our study, to reflect normal processes of healthy brain development as much as possible. Clinical description and the availability of DWI/rs-fMRI data of the included neonates are presented in Table 1.

Scan Preparation and Sedation

Prior to MR scanning all infants were sedated; chloral hydrate was administered orally (50–60 mL/kg). To minimize motion during scanning, all neonates were immobilized by wrapping them into a vacuum cushion. MiniMuffs (Natus Europe, Münich, Germany) and earmuffs (EM's kids,

Table 1
Demographics

Neon	Gender	GA	PMA	PMA	DWI		RS		Twin	BW	IUGR	HYP	PDA	BPD	Sepsis	IVH	GMI	WMI	Other lesions
			30	40	30	40	30	40											
1	F	27.9		41.7		X		X		780		X							
2	M	27.1		42.3		X		X		565	X			X	X				
3	F	24.6	31.4	40.6	X	X	X	X	X	870			X			2	Mild		<6 PWML
4	M	27.9	30.9	41.0	X	X	X	X	X	460	X							Mild	
5	M	27.1	31.6	41.7	X	X	X	X		950			X				Mild		
6	M	26.7	31.3	40.3	X	X	X	X		640					X				
7	F	27.3		41.4		X		X		995									
8	F	27.9	30.0	41.3	X	X	X	X		960		X	X					Mild	
9	F	25.7		40.7		X		X		870			X			2		Mild	
10	M	24.1		40.7		X			X	685			X	X		2			
11	M	26.1	30.0	41.0		X	X	X	X	975							Mild	Mild	
12	F	27		41.4		X		X		755			X		X				
13	M	29.4		40.7		X		X		1360								Mild	≥6 PWML
14	M	27.9	31.1	41.0			X	X		1110			X					Mild	<6 PWML
15	F	27.3	31.9	41.9		X				570	X		X	X	X		Mild	Mild	
16	M	30.6	31.4	41.6	X	X		X		930	X	X	X					Mild	≥6 CBH
17	F	27.7	31.1	41.4	X	X				680			X	X				Mild	<6 PWML, <6 CBH
18	F	27.1	29.9	41.0		X		X		1020					X				
19	F	27.4	30.0	40.4	X					895			X		X			Mild	
20	F	27.6	29.7	40.6		X		X		1000							Mild	Mild	
21	F	27.9	29.9	40.9	X		X		X	1000					X			Mild	
22	M	27.9	30.9	40.9	X		X		X	1295				X				Mild	
23	F	25		41.3		X				810		X	X	X	X	2		Mild	<6 PWML, ≥6 CBH
24	M	24.7		41.0		X				700			X	X	X			Mild	
25	F	29.4	30.1				X			1215									<6 PWML, <6 CBH
26	M	25.1	30.0				X			680						2	Mild	Mild	<6 CBH
27	M	25.3	31.6				X			740				X				Mild	<6 PWML
Total No Mean (SD)	13/14	27.0(1.6)	30.8 (0.7)	41.2 (0.5)	10	20	20	16	6	871 (222)	4	4	13	8	9	5	6	17	6 <6 PMWL 1 ≥ 6 PWML 3 < 6 CBH 2 ≥ 6 CBH

Imaging data of 36 neonatal datasets from 27 neonates with MRI around week 30 and week 40 postmenstrual age (PMA) were included; serial measurements at both 30 and 40 weeks PMA were available for 9 neonates. Neon, neonate; GA, gestational age at birth; PMA, postmenstrual age (weeks) at time of scan; DWI, diffusion-weighted imaging data were acquired and of sufficient quality; RS, resting-state data were acquired and of sufficient quality; Twin, part of a twin; BW, body weight at birth (in grams); IUGR, intrauterine growth restriction defined as birth weight below p10; HYP, hypotension requiring inotropes and/or vasopressors; PDA, patent ducus arteriosus requiring therapy; BPD, bronchopulmonary dysplasia (defined as oxygen dependency at 36 weeks PMA); sepsis, blood culture proven sepsis; IVH, intraventricular hemorrhage (scored according to Papile et al. (1978)); WMI, white matter injury; GMI, gray matter injury; mild, mild injury; PWML, punctate white matter lesions; CBH, punctate cerebellar hemorrhages; No, number of patients; SD, standard deviation; X, yes; F, female; M, male. GMI and WMI were graded according to the white and gray matter injury scores of Woodward et al. (2006).

Everton Park, Australia) were used to reduce noise and for further stabilization. Throughout the examination, the following parameters were monitored; heart rate, respiratory rate, and transcutaneous oxygen saturation. A neonatologist was present at all time during the examination.

Anatomical T_1-Weighted Image

Acquisition

A T_1-weighed image (3D Fast Field Echo using parallel imaging; TR/TE 9 ms/4.6 ms; field of view (FOV) 200 × 200 mm, 110 slices, 0.78 × 0.78 × 1.2 mm voxelsize, 30 weeks: TR/TE 9.4 ms/4.6 ms, 0.94 × 0.94 × 2.0 mm voxelsize) was acquired for anatomical reference.

Image processing

A neonate anatomical template (Oishi et al. 2011) was registered to the neonatal T_1 image, and the 56 cortical regions of the template were selected as regions of interest. A detailed description of this neonatal template, including information and illustrations on the 56 regions and an open access copy of the template, is presented in the paper of Oishi et al. (2011).

Diffusion Weighted Imaging

Acquisition

A DWI set of 32 weighted diffusion scans ($b = 800$ s/mm^2) and an unweighted B0 scan ($b = 0$ s/mm^2) were acquired (DWI-MR using parallel imaging SENSE P-reduction 2; TR = 5764 ms, TE = 70 ms, FOV 180 × 146.25 mm, voxel size 1.4 × 14 × 2.0 mm, 50 slices).

Image processing

Processing included the following steps: DWI images were 1) corrected for eddy-current distortions and small-head movements (Andersson and Skare 2002) and realigned to the $b = 0$ image. 2) The diffusion profile of each voxel was fitted a tensor using a robust tensor fitting method (Chang et al. 2005), and 3) the principal eigenvector of the eigenvalue decomposition of the fitted tensor was taken as the main diffusion direction within each voxel. 4) Using the results of the eigenvector decomposition, several metrics of microstructural organization of white matter were computed (Beaulieu and Allen 1994; Jones 2008), including the level of fractional anisotropy (FA), a metric of microstructural organization and often used as an estimate of the level of white matter integrity, the level of mean diffusion (MD), an estimate of the total level of diffusion within a voxel, the level of transverse diffusion (TD), reflecting the amount of restricted diffusion in the perpendicular direction of the first eigenvector and, in the adult brain, often interpreted as an (inverse) estimate of the level of myelination of white matter, and the level of parallel diffusion (PD), a metric of the level of local fiber orientation.

Reconstruction of White Matter Tracts

Streamline tractography based on the Fiber Assignment by Continuous Tracking algorithm (FACT) (Mori and van Zijl 2002) was used to reconstruct the white matter pathways of the neonatal brain. To this end, within each voxel eight seeds were started, and the main diffusion direction was followed from voxel to voxel, until one of the stopping criteria was met, being when the streamline reached a voxel with a low FA value (<0.1), when a streamline left the brain mask or when a reconstructed streamline made a sharp turn (>60°).

Resting-State fMRI

Acquisition

Measurements of endogenous brain activity of the neonatal brain were acquired through means of the acquisition of 6.71 min (256 volumes) of resting-state fMRI (parameters: 2D EPI SENSE, TR/TE 1600/45 ms, flip-angle 50; SENSE reduction 2, 2.5 mm isotropic voxel size, 22 consecutive slices covering the whole neonate cortex).

Image Processing

Imaging processing steps were performed using SPM8 (www.fil.ion.ucl.ac.uk/spm/software/spm8). Time-series were realigned and co-registered with the T_1 image to ensure overlap with the cortical ROI template. Voxel-wise time-series were 1) de-trended (removing linear trends and first order drifts), 2) corrected for global effects (regressing out white matter, ventricle, and global mean signals). To minimize potential influences of motion-induced spurious effects into FC the effects of motion (as assessed through means of the 6 motion parameters resulting from image realignment) were also regressed out of the resting-state time-series. No significant differences were observed in the motion parameters between the 30-week and 40-week datasets (all $P > 0.05$). Considering recent concerns of motion-related artifacts introducing spurious effects into FC, several steps were undertaken to minimize the effects of motion in our FC analysis (van Dijk et al. 2011; Power et al. 2012; Satterthwaite et al. 2013): All neonates were sedated during scanning, which minimizes the effects of voluntary head movement, and all neonates were fixated in place by means of foam paddings, straps, and/or a vacuum cushion. Across datasets, no significant differences were found in motion parameters between 30- and 40-week neonates. The functional time-series were "scrubbed' before FC computation (i.e., removing scans that showed a frame-wise displacement of >0.5 mm, as proposed by Power et al. (2012). Scrubbing resulted in the exclusion of (mean/standard) 9.75%/13%). In 2 neonates, more than 33% of the scans showed more than 0.5 mm displacement (52 and 35%). Removing these 2 neonatal datasets did not change the nature of the resting-state findings. 3) Time-series were band-pass filtered (0.01–0.1 Hz) to select resting-state frequencies of interest.

Structural Connectome Reconstruction

The brain's network was mathematically described as a graph, describing a collection of nodes, and a collection of connections (also called edges) of the network. Nodes were selected as the cortical regions of interest of the neonate template (Oishi et al. 2011), resulting in a parcellation of the whole neonate cerebral cortex into 56 regions (25 cortical regions covering each hemisphere, together with bilateral amygdala, hippocampus, and cerebellum). Network nodes were defined as being structurally connected when a set of tractography streamlines was present in the total collection of reconstructed streamlines that interconnected them, with the number of reconstructed streamlines taken as an indirect measure of white matter volume. In addition to using absolute streamline count as a connectivity metric, additional analysis were performed in which more qualitative weights of connectivity were taken, including the level of FA as a metric of overall white matter integrity (e.g. van den Heuvel et al. 2010).

The neonatal (and adult, see below) brain network was reconstructed at a relative low spatial resolution, examining structural and FC between large-scale brain regions, of varying sizes. Other studies have shown the feasibility of reconstructing and examining brain networks at higher resolutions (e.g., Eguiluz et al. 2005; Hagmann et al. 2008; van den Heuvel et al. 2008; Bassett et al. 2010; Zalesky et al. 2010; van den Heuvel and Sporns 2013). The optimal resolution for MRI-based connectome reconstruction and examination remains, however, unknown (de Reus and van den Heuvel 2013). At lower resolutions, subtle connectivity effects might be missed due to spatial averaging, but higher resolution parcellation schemes have been shown to involve higher levels of intersubject variability, making the accumulation of information into group-averaged connectome maps and perform between-group analysis more difficult (de Reus and van den Heuvel 2013).

Functional Connectivity and Functional Networks

For each neonatal dataset, the level of FC between all pairs of nodes in the network was assessed through means of a correlation analysis. To this end, for all regions a regional averaged resting-state time-series was computed, as the average time-series of all voxels within a region. Next, between all pair of cortical regions the level of correlation between their region time-series was computed, resulting in FC matrix describing the level of cortico-cortical interregional functional couplings between each pair or regions in the neonatal brain. Negative correlations were included and interpreted as low functional interactions between brain regions (Hagmann et al. 2008; van den Heuvel et al. 2012, 2013).

Next, a group-averaged FC matrix was created by averaging the individual FC matrices across all individuals, and the formation of functional communities -also referred to as resting-state networks- was examined by means of modular decomposition of this group-averaged

FC matrix (Rubinov and Sporns 2010, 2011). For this analysis, negative weights were set to 0.

Group-Averaged Connectomes

Group-averaged structural and functional connectomes were computed for the total group of neonates, and for the week 30 and week 40 groups separately. Structural group connectomes were formed by including structural connections that were presented in 60% or more of the total group (de Reus and van den Heuvel 2012), with the weights of the connections in the group connectome taken as the mean of the values across the included individuals. Similar, group-averaged functional connectomes were computed as the average of the FC values across the group of subjects.

Graph Theory

Characteristic graph metrics were computed to describe the topological organization of the neonatal structural connectome. Graph metrics were computed based on both the individual unweighted networks (main analysis) and on the weighted networks (FA-weighted, additional analysis). Metrics included (see also Supplementary Materials):

1. *Clustering coefficient C*, describing the level of topological local connectedness of a node. The overall clustering coefficient C was computed as the mean of C_i over all nodes i in the network. The normalized clustering coefficient γ was computed as the ratio between C and the mean clustering coefficient C_{random} of a set of random networks (1000 networks, randomizing the connections of the original network, keeping the degree sequence intact (Maslov and Sneppen 2002)).
2. *Shortest path length L*, describing the average minimal travel distance between nodes in the network. The overall path length L was computed as the mean of shortest path length L_i over all nodes i in the network. The normalized path length λ was computed as the ratio between L and the mean shortest path length L_{random} of a set of random networks (1000 networks, randomizing the connections of the original network, keeping the degree sequence intact (Maslov and Sneppen 2002)).
3. *The small-world index SW* was computed as the ratio the normalized clustering coefficient γ and the normalized path length λ, with SW >1 indicating a small-world organization of a network (Humphries et al. 2006).
4. *Modularity Q*, describing the tendency of the network to be formed out of distinct, separated communities, each characterized by high within-community connectivity and relative low connectivity to other communities. Modularity was computed on basis of Newmann's community detection algorithm (Newman 2006).
5. *Rich club organization*, describing the tendency of high-degree nodes in the network to be densely interconnected, above what one would expect on the basis of their degree alone (Colizza et al. 2006). Following recent reports of rich club organization of the adult connectome (e.g (van den Heuvel and Sporns 2011)), rich club organization of the neonatal connectome was computed as follows: For the group-averaged neonatal connectome, for each level of degree k the rich club coefficient $\Phi(k)$ was computed as the ratio between the number of connections present within the subset of nodes $E_{>k}$ with a degree of $>k$, and the number of connections that could maximally be present between the nodes in $E_{>k}$. A network displays a rich club organization if, for a range of k, $\Phi(k)$ exceeds the rich club coefficient $\Phi_{\text{random}}(k)$ of a set of random graphs exceeds 1. The normalized rich club coefficient $\Phi_{\text{norm}}(k)$ is defined as the ratio between $\Phi(k)$ and $\Phi_{\text{random}}(k)$. In this study, a set of 1000 random networks was formed by randomizing the connections of the group-average neonatal connectome, maintaining an identical level of overall sparsity, as well as preserving the degree sequence of the network (i.e., hubs remain hubs), but with the underlying network organization randomized.

Integration Capacity Between Resting-State Communities

Integration capacity. The level of integration capacity of a network measures the capacity of the network to integrate information between its communities. Given a network X, with n functional modules (here taken as the 4 functional networks, see Results), the level of integration $I(X)$ of the network as a whole can be computed through means of information theory. A mathematical description of $I(X)$ is given in the Supplemental Materials and in (Zamora-Lopez et al. 2010). In short, $I(X)$ measures the capacity of the network to integrate information between its segregated communities. A system with total independence between its modules satisfies $I(X) = 0$. Increasing levels of $I(X)$ indicate a higher capacity of the structural connections of the system to integrate information between its subparts. As communities were defined on basis of module decomposition of the FC matrix, $I(X)$ here reflects the level of integration between functional domains of the brain system.

Adult Connectome

The neonatal connectome (both structurally and functionally) was compared to the adult connectome. The adult connectome was taken from a dataset as described in detail in Collin et al. (2014). This dataset included data from 26 males and 16 females (age mean/standard: 29/8.0 in years). The adult connectome resulted from a reconstruction of the adult brain network on basis of DWI, resulting in a macroscopic connectome describing all cortical-cortico white matter connections between 68 cortical regions. For comparison to the neonatal connectome, the 68 regions of the adult connectome were manually overlapped with the regions provided in the Oishi atlas (Oishi et al. 2011). The adult connectome included a more detailed parcellation of the human cortex (68 cortical regions vs. 50 cortical regions (subcortical and cerebellum were excluded when comparing to the adult cortical conenctome) in the neonatal connectome). To match the cortical regions as defined in the neonatal atlas, cingulate regions (posterior, anterior, caudal, isthmus cingulate), rostral frontal regions (rostral middle frontal, rostral caudal middle frontal, frontal pole), lateral frontal (parsopercularis, parsorbitalis, parstriangularis), and lateral temporal (superior temporal, transversetemporal and temporal pole) were merged together into single cortical regions, respectively.

Statistical Analysis

Comparison of the Layout of the Neonatal and Adult Connectome

The connectivity layout of the group-averaged neonatal SC and FC brain networks were compared with the connectivity layout of the SC and FC adult brain networks. An adjusted version of the Mantel test for comparison of matrices was used (Mantel 1967). First, for the SC and FC matrices, the overlap between the binary neonatal and adult group-averaged matrices was compared, yielding a "distance matrix" (DIS) indicating for each cell entry whether the cell entries were similar or different across the neonatal and adult matrix. When cell entries were overlapping across the neonatal and adult connectome, this was marked as a 1 in the DIS matrix, and 0 otherwise. Second, the total level of overlap O was expressed as the level of sparsity of the DIS matrix (i.e., the percentage of entries being a 1 present in the DIS matrix), ranging between 0% (no overlap between the neonatal and adult matrix, showing maximal distance between the 2 matrices) and 100% (complete overlap between the neonatal and adult matrix, indicating minimal distance between the 2 matrices). Third, similar to the Mantel test, permutation testing was used to obtain a null-distribution of distance scores that are present under the null-hypothesis of no overlap being present between the 2 matrices. To this end, for each permutation, the entries of neonatal and adult connectome were randomized (obtaining a similar degree distribution (Maslov and Sneppen 2002)) and a DIS* matrix was computed, together with the overlap score O*. This was repeated for 10 000 permutations, yielding a null-distribution of O*. Fourth, the original overlap score of the neonatal and adult matrix was assigned a P-value as the percentage of the obtained null-distribution that exceeded the original overlap score (van den Heuvel et al. 2010, 2013). For the comparison of the FC matrices, suprathreshold FC correlations of $>T$ were used. Multiple settings of T ($0 < T < 0.2$) were tested (see Results).

Developmental Effects

Developmental effects of white matter changes and graph metrics were examined through means of cross-sectional analysis using linear regression, with GA as the independent variable and white matter integrity/graph metrics as the dependent variable of interest. Longitudinal effect was examined by means of two-sample tests.

Results

In what follows, we describe results pertaining the architecture of the neonatal connectome, including a description of its structural and functional organization, followed by results pertaining the development of neonatal connectivity during the first weeks (week 30 to week 40 corrected GA) of cerebral connectome genesis.

Topological Organization of the Structural Neonatal Connectome

For each individual dataset, a structural brain network was formed on the basis of the diffusion-weighted data, reconstructing the cortico-cortical tracts of the neonatal brain. Examining the (binary) topological organization of the resulting network, revealed high levels of binary clustering (mean/standard: 0.66/0.033) and normalized clustering (1.46/0.25, when compared with 1000 random networks), suggesting a high level of local organization, higher than one can expect on basis of a random topology (Fig. 1*a*). Furthermore, networks revealed overall short communication paths (mean/standard: 1.70/0.11, normalized: 1.04/0.030, 1000 networks). Taken together, such an efficient local and global organization is indicative of a small-world organization of the preterm neonatal brain (small-world index, mean/standard: 1.40/0.20, 1000 random networks) (Fig. 1). Incorporating information on the weights of the connections on the basis of the number of streamline count (NOS) and FA revealed similar findings, showing above chance levels of clustering and overall short communication paths in the neonatal brain. Consistent with the observed clustering, the neonatal structural connectome revealed high levels of modularity Q (mean/standard: 0.27/0.06), significantly higher than a level of modularity that one would expect on the basis of a random network ($P < 0.001$).

Connectivity Hubs

In addition to a small-world modular topology, the neonatal connectome revealed a right-tailed degree distribution (Fig. 1*b*), suggestive of the existence of a small number of densely connected "hub nodes." Such an organization overlaps with reports of hub formation in the adult brain (van den Heuvel and Sporns 2013). The top 12 (20% of total) of highest connected nodes included left superior frontal cortex, left lateral front-orbital gyrus, left precentral gyrus, left postcentral gyrus, left and right superior parietal lobule, left and right cingular gyrus, left and right angular gyrus, and left and right fusiform gyrus (Fig. 1*c*). Notably, the network betweenness centrality of these high-degree nodes was found to be significantly higher than that of nonhigh-degree nodes ($P < 0.001$, 10 000 permutations), suggesting a central position of these nodes in the overall network topology. Besides being individually "rich" in connectivity, these putative brain hubs showed an above chance level of interconnectivity, which suggest the presence of a densely connected central "core" or "rich club" in the neonatal brain, a type of network organization reported for the adult human connectome (van den Heuvel and Sporns 2011). Figure 1*d* shows the rich club curve of the neonatal

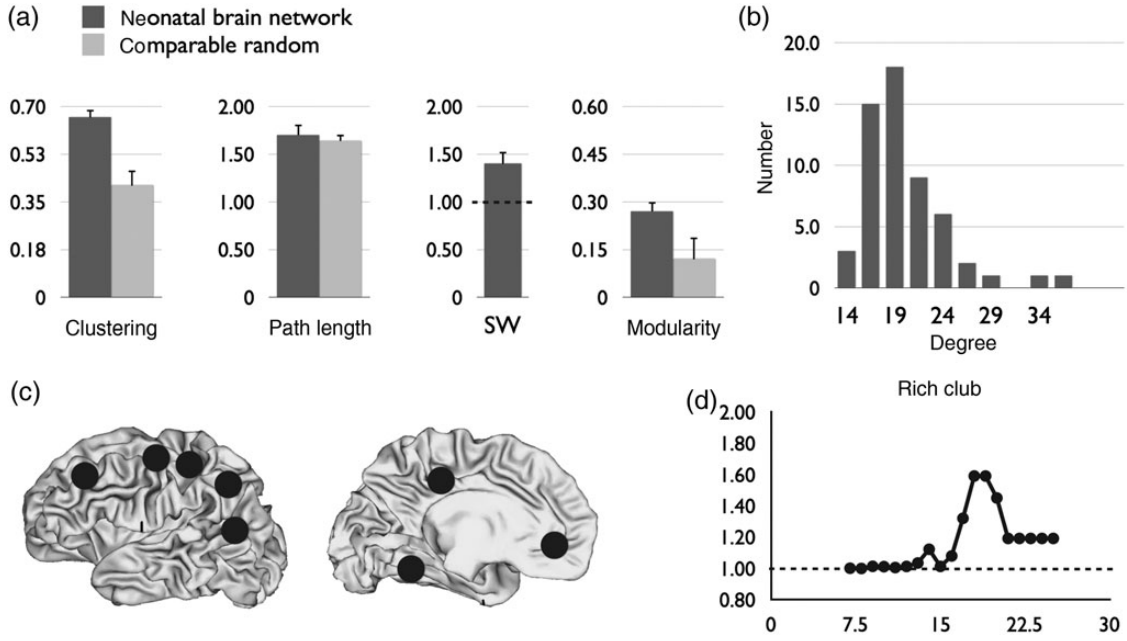

Figure 1. Network descriptive of the neonatal connectome. (*a*) "Small-world organization of the neonatal brain." Figure shows the clustering coefficient and shortest path length values of the individual neonatal connectome (dark gray bars) and levels of a set of comparable networks (light gray). Error bars depict variation (standard deviations) across the individual datasets. The small-world index SW was significantly higher than 1, suggesting a small-world organization of the neonatal connectome at term. (*b*) "Degree distribution." Figure shows a right-tailed distribution of the group-averaged connectome, indicating the existence of high-degree hub nodes in the neonatal brain. (*c*) "Hubs." Figure illustrates the locations of the top 12 high-degree hub nodes in the group-averaged neonatal connectome (locations are shown on one hemisphere only, yielding 8 unique hub locations, see Results). (*d*) "Rich club organization." Rich club analysis revealed above rich club coefficient levels >1, indicating dense levels of connectivity between high-degree nodes, as previously reported for the adult connectome.

connectome (group-average) with the normalized rich club coefficient $\Phi_{norm}(k) > 1$ for the range of $k > 17$ and $k > 24$, indicative of a dense level of connectivity between high-degree nodes of the neonatal brain and suggestive of the formation of an early rich club collective in the neonatal connectome.

Functional Connectivity and Functional Networks of the Neonatal Brain

Functional connectivity of the neonatal brain was examined by means of correlation analysis between resting-state fMRI time-series of cortical brain regions. Cortical regions were identical to the nodes of the structural network, allowing for a direct overlap between the structural (SC) and functional (FC) connections of the neonatal brain. Figure 2*a* shows a side-by-side comparison of the group-averaged FC matrix of the neonates, together with the group-averaged SC matrix. Rows and columns of both the FC and SC matrix are arranged in the same ordering, with the nodes arranged according to FC module participation (Fig. 2*b*), showing a clear overlap between the neonate's functional and structural connectivity layout.

Functional Networks

Functional networks showed a modular organization ($Q = 0.40$). Across the group of neonates, 4 functional modules could be identified, describing a (bilateral) 1) frontal network, a 2) motor/sensory network, an 3) occipital visual network and a 4) temporal/auditory network.

Structural–Functional Coupling

The level of structural–functional coupling was examined through means of Pearson correlation analysis. Structural weights (NOS count) of the non-zeros entries of the network were rescaled to a Gaussian distribution and correlated with their functional counterparts, resulting in a single structure–function coupling (SC-FC) metric (Hagmann et al. 2008; Honey et al. 2009; Collin et al. 2014). A positive SC-FC coupling was found to be present in all neonates, suggesting that higher levels of structural connectivity are associated with higher levels of functional coupling (SC-FC coupling, mean/standard: 0.31/0.089).

Comparison of the Neonatal Brain Network to the Adult Connectome

Structural Connectome

To examine whether particular structures of the adult human connectome are already present at (term equivalent) birth, the organization of the neonate's connectivity circuitry was compared with the organization of the connectome of a group of adults. An adult connectome was reconstructed based on DWI data from a group of healthy adult participants (see Materials and Methods for details). Figure 3*a* shows a side-by-side comparison of the neonatal connectome and a group-averaged adult connectome, illustrating a high level of overlap between the network of the neonatal brain (left panel) and that of the adult brain (right panel) on SC. For visual comparison, regions

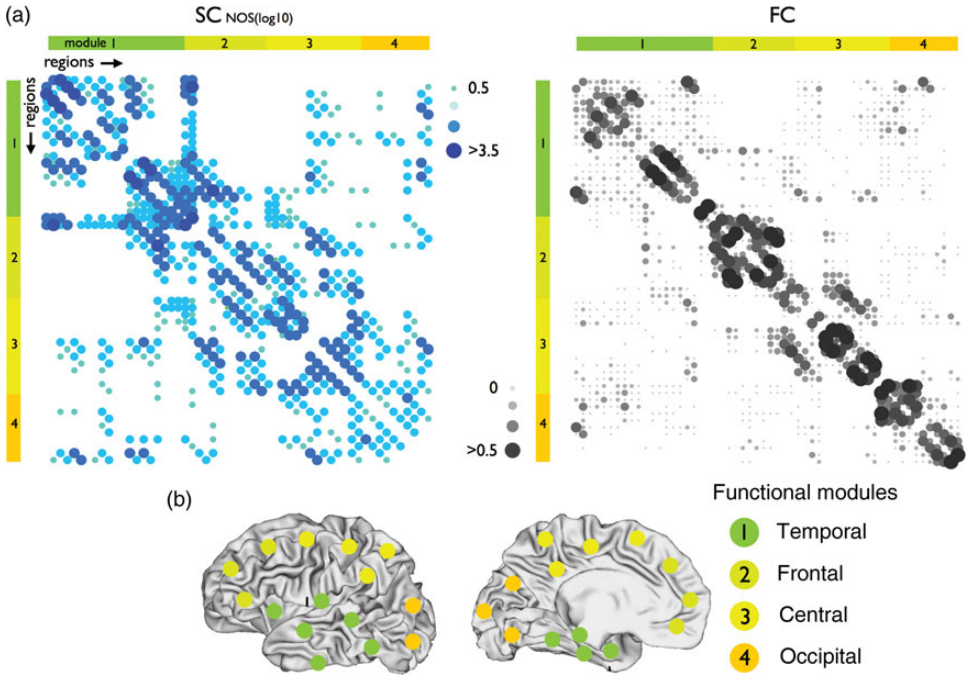

Figure 2. Structural and functional connectivity matrices of the neonatal connectome. Figure shows the structural and functional connectivity matrices of the group-averaged neonatal brain. Rows and columns include all cortical regions, expressing the level of structural and functional connections between each pair of regions in the neonatal brain. The structural connectivity matrix (SC) is shown in the left panel, with the levels of connectivity expressed as the number of reconstructed streamlines (NOS) between each pair of regions. Higher levels of SC are indicated by larger dots. Levels of positive functional coupling (i.e., functional connectivity, higher levels of FC are indicated by larger dots) between each pair of regions are shown in the functional connectivity (FC) matrix as shown in the right panel. The columns and rows (i.e., nodes of the network) are ordered according to the community assignment as based on community detection on the FC matrix (see Materials and Methods) revealing the existence of 4 functional communities in the neonatal brain. These communities overlapped temporal (auditory regions), occipital (visual regions), central (motor and sensory regions) and frontal cortex. Distribution of the nodes across the cortex are illustrated in the lower panel. Figure illustrates clear overlap between the SC and FC matrix of the neonatal brain, indicating a structural basis of functional connectivity in the neonatal brain. To aid visual comparison between the SC and FC matrices, positive values are shown in the FC matrices with all negative correlations represented as empty cells.

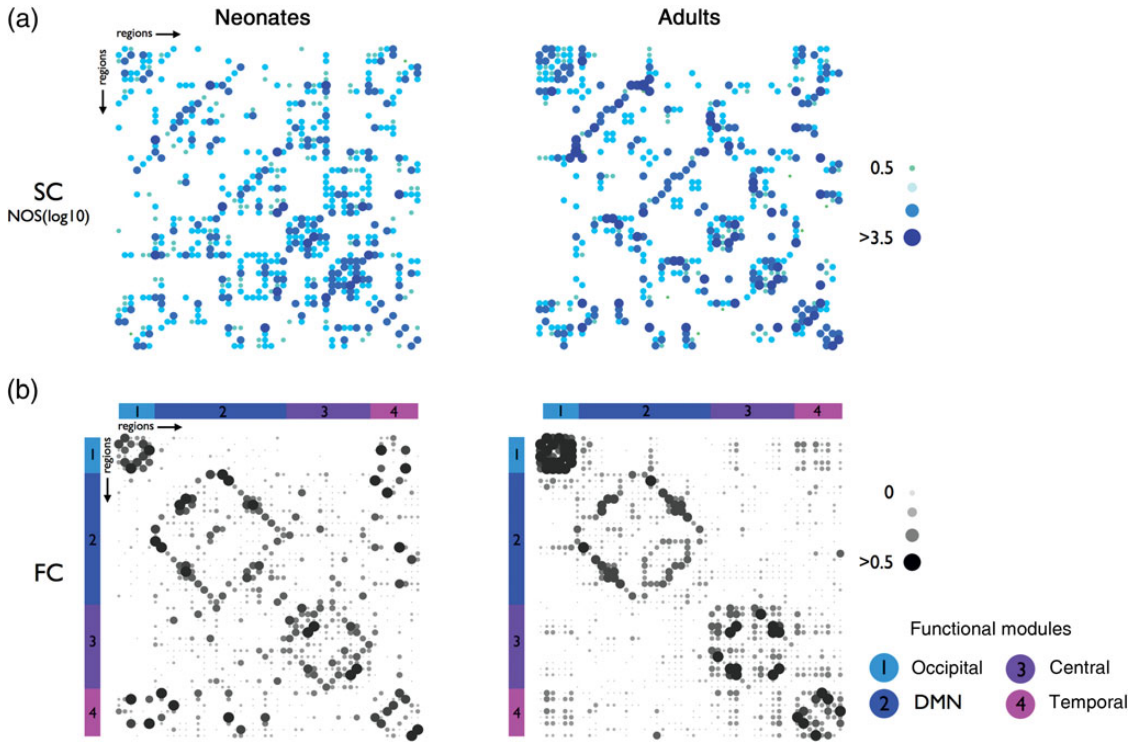

Figure 3. Comparison of the group-averaged neonatal and adult connectome. Upper panels show the structural connectivity (SC) matrices (NOS weighted) of the neonatal (left) and adult (right) group-averaged connectome. Rows and columns (i.e., nodes of the network) are ordered according to the community structure of the adult FC matrix. Lower panels show the level of positive functional coupling (functional connectivity FC) between each pair of regions in the neonatal (left) an adult connectome (right). Columns and rows (nodes) of the matrices are ordered according to module decomposition of the adult functional connectome, revealing 4 distinct functional modules, overlapping an occipital (visual), temporal (auditory), central (sensory, motor network) and the functional default mode network. Figure shows overlap between both the SC matrices of the neonatal and adult group (overlap: 81%, see Results), confirming our observations that overall SC structure is present before term equivalent birth. Furthermore, overlap between the FC matrices (overlap: 79%, see Results) suggests the presence of outlines of functional modules in the neonatal brain, albeit being in an immature state. Note that the rows and columns (i.e., nodes of the network) are ordered according to the community structure of the adult FC matrix, and thus different from the ordering used in Figure 2.

of the neonate and adult template are placed into the same arrangement to allow a visual comparison between the 2 networks (see Materials and Methods), showing clear overlap between the structural of the neonatal and adult connectome. Quantitative comparison of the group-averages structural neonatal and adult connectome (comparing the existence and nonexistence of each of the entry in the matrix between the group-averaged neonatal and adult structural connectivity matrix) revealed 84.6% overlap between the 2 matrices ($P < 0.001$, 1000 permutations). Importantly, focusing on the intrahemispheric connections in the neonatal and adult connectome (i.e., cortico-cortical connections within a single hemisphere, not taking into account interhemispheric corpus callosal tracts) also showed a high level of overlap (76% averaged over the 2 hemispheres, $P < 0.00$, 1000 permutations; left hemisphere: 78% right hemisphere: 75%). These results are indicative of the majority of all large-scale pathways (both intra as well as interhemispheric tracts) to be present at term, together with an adult-like small-world modular architecture.

Functional Networks

Figure 3*b* shows a side-by-side comparison of the FC matrix of the group of neonates and the group of adults. Rows and columns (i.e., nodes of the network) are arranged in the same ordering as the matrices in Figure 3*a*. Side-by-side comparison again shows that the FC matrix of the neonatal group shows the same contours of the community structure of the adult matrix, suggestive of the notion that the outlines of "adult-like" functional networks are already present (albeit in an underdeveloped form) directly from the first phases of connectome formation. Quantitative comparison of the existence and nonexistence of (suprathreshold FC connections using a $T > 0.1$) functional connections in the adult and neonatal connectome revealed 81% overlap between the 2 matrices ($P < 0.001$, 1000 permutations). Intrahemispheric FC connections was also found very consistent across adult and neonatal networks (77% averaged over the 2 hemispheres, $P < 0.001$, 1000 permutations; left hemisphere: 77%, right hemisphere: 77%). Different thresholds T resulted in similar findings (whole brain: $T > 0$: 62% $P < 0.001$, $T > 0.2$: 86% $P < 0.001$; intrahemisphere (averaged over 2 hemispheres): $T > 0$: 62% $P < 0.001$, $T > 0.2$: 86% $P < 0.01$, all tests survived Bonferroni correction for multiple testing).

Development of the Neonatal Connectome

Acquisition of MR data at 2 different periods of GA (28–32 and 40–42 weeks) allowed for an exploratory analysis of early developmental changes of the connectome. Our cross-modal structural–functional study design allowed for the examination of at least 4 aspects of development, including an examination of 1) developmental changes in microstructural white matter organization, 2) effects of white matter changes on the topological organization of the macroscopic neonatal connectome, 3) developmental influences on the formation of functional

networks, and 4) conjectural implications of connectome development on the communication and integration efficacy of the neonatal brain network.

Preterm Development of White Matter Structure

Examination of the white matter markers between week 30 and week 40 postconceptional age revealed changes in prenatal white matter microstructure. First, FA showed a significant increase over time ($r = 0.90$, $P < .001$, Fig. 4*a*), suggesting a development of the local microstructure of the brain's structural connections. Second, other markers of white matter efficacy also showed a clear association with age, including a developmental decrease in the MD ($r = 0.88$, $P < 0.001$, Fig. 4*a*), a decrease in TD coefficient ($r = 0.88$, $P < 0.001$, Fig. 4*a*), and decrease in the PD coefficient ($r = 0.82$, $P < 0.001$). As the age range was not normally distributed, additional statistical testing was performed to verify the significance of these findings: Directly testing group differences on FA, MD, TD, and PD between the group of 30-week GA neonates (<32 GA) and the group of 40-week GA neonates (>38 GA) using nonparametric permutation testing of the 2 group means all revealed significant differences between week 30 GA and week 40 GA neonates ($P < 0.001$, 10 000 permutations). (All tests survived Bonferroni correction for multiple testing).

Longitudinal Analysis

The increase in white matter microstructure was confirmed in the longitudinal analysis (7 neonates were scanned both around 30 weeks and around 40 weeks), showing a significant increase in FA ($P < 0.001$, Fig. 6) and a significant decrease in MD ($P = 0.005$, Fig. 6), TD ($P < 0.001$), and PD ($P = 0.0014$). All tests survived Bonferroni correction for multiple testing.

Development of the Topological Architecture of the Neonatal Connectome

Next, we examined the effects of white matter changes on the development of the topological properties of the brain's network circuitry. A positive increase in clustering coefficient C was observed ($r = 0.78$, $P < 0.001$, Fig. 5*a*), together with shorter communication pathways, as shown by a decrease in total path length L ($r = 0.83$, $P < 0.001$, Fig. 5*a*). Normalized to the organization of a set of 1000 random networks, white matter development coincided with an increase in the overall small-world organization of the network ($r = 0.47$, $P = 0.006$, Fig. 5*b*), suggestive of the growth of the neonatal connectome to a more overall efficient organization during development. In addition, coinciding with the increase in clustering, also the level of modularity of the network was found to increase between 30 and 40 weeks ($r = 0.50$, $P = 0.0037$, Fig. 5*b*). The tests of C, L, and SW survived Bonferroni correction for multiple testing.

Longitudinal Analysis

The impact of development of white matter microstructure on network topology was confirmed in the longitudinal analysis, showing a modest increase in the network's small-world organization of the neonatal connectome between 30 and 40 weeks ($P = 0.006$, Fig. 6), together with an increase in normalized clustering ($P = 0.014$).

Preterm Development of Functional Resting-State Networks and Structural-Functional Coupling

No clear developmental increase in overall FC (i.e., averaged over all connections in the FC matrix) was observed between week 30 and week 40 GA. A significant increase in interhemispheric FC (aggregated over all homotopic left-right hemispheric region pairs, as an often examined metric of positive

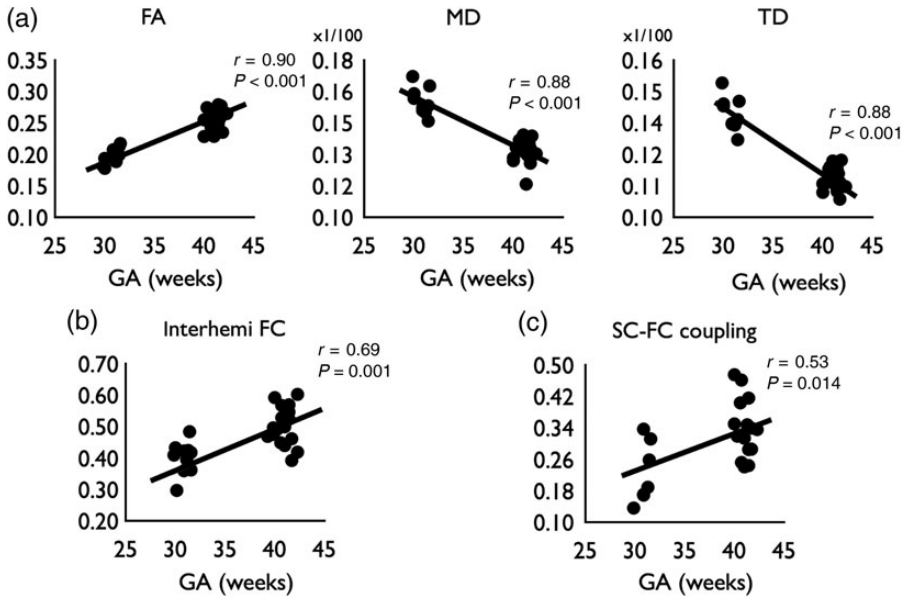

Figure 4. Development of structural and functional connectivity (*a*) Panels show individual levels of fractional anisotropy (FA), mean diffusivity (MD) and transverse diffusivity (TD) of each included neonatal dataset in relationship to age. Panels show a clear increase in white matter development between week 30 and week 40 gestational age (GA), illustrated by an increase in FA and a decrease in MD and TD over time. (*b*) Panel shows individual levels of interhemisperic functional connectivity. (*c*) Developmental change of structural - functional coupling between week 30 and week 40 GA.

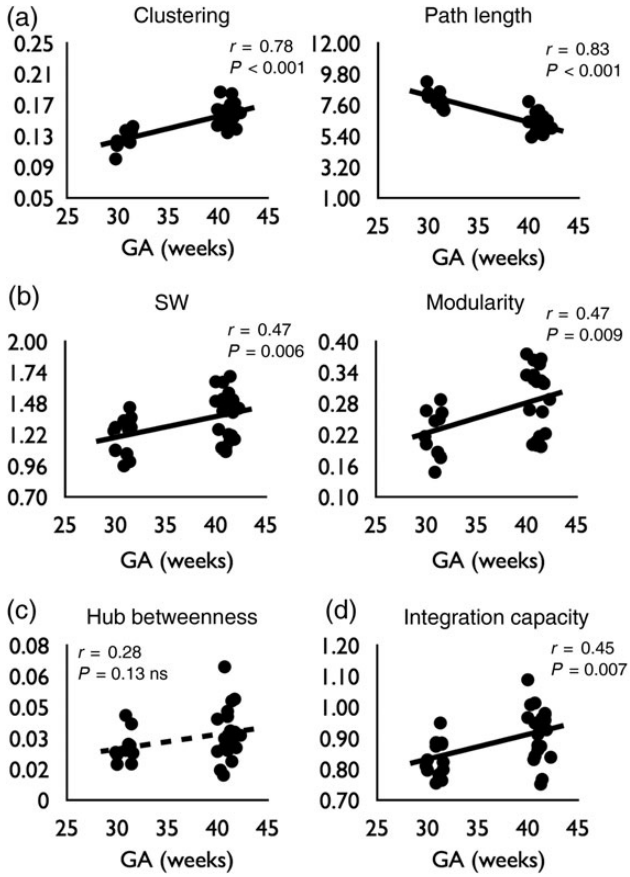

Figure 5. Development of network characteristics. Figure shows individual levels of several network characteristics of the (unweighted) structural neonatal brain network between 30 and 40 weeks gestational age (GA). (*a*) The level of clustering C was found to significantly increase over time. Furthermore, the level of path length L was found to decrease over time, indicating the formation of shorter communication pathways in the neonatal brain. (*b*) The increase in clustering and decrease in path length resulted in a significant increase in small-world topology of the neonatal brain between week 30 and week 40. Neonatal development was also found to involve an increase in network modularity, suggesting a sharper definition of structural modules in the neonatal brain over time. (*c*) Hub nodes (see Materials and Methods, and Fig. 1) in the neonatal brain network were only found to show, at best, a marginal increase in centrality over time. This effect was not significant ($P = 0.13$ ns). (*d*) The level of Integration Capacity (as estimated by mathematical modeling on basis of the structural connectivity network) was found to increase between week 30 and week 40 GA.

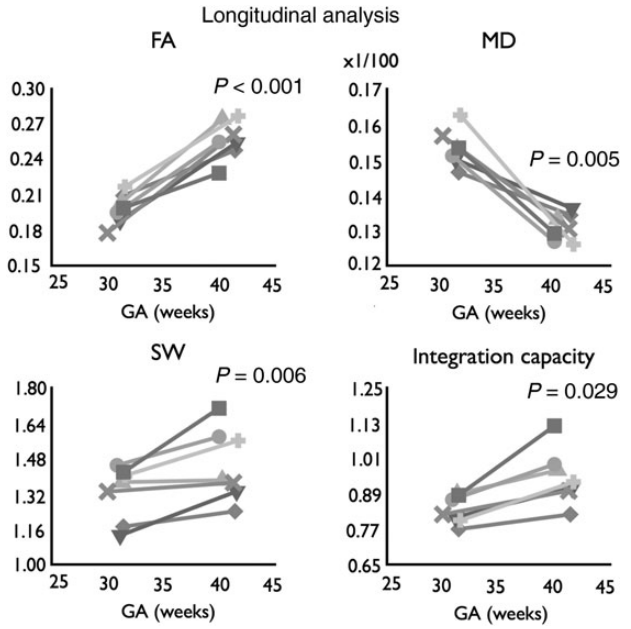

Figure 6. Development of structural connectivity and network characteristics (longitudinal analysis). Of 7 neonates, longitudinal assessment of brain development was possible, on the basis of a structural and functional MRI measurement at both (around) week 30 and week 40 gestational age (GA). Longitudinal analysis confirmed developmental changes in structural and functional properties of the neonatal brain network. White matter microstructure showed a clear development between week 30 and week 40 GA in all 4 neonates, including a significant increase in fractional anisotropy (FA), a decrease in mean diffusivity (MD) of white matter and an increase in small-world (SW) properties of the network. Furthermore, confirming the cross-sectional findings, integration capacity showed a significant increase during week 30 and week 40 GA.

functional couplings in resting-state fMRI studies) was observed between week 30 and week 40 GA ($r = 0.69$, $P = 0.001$, Fig. 4*b*). Intrahemispheric FC (aggregated over all intrahemispheric connections) was not found to significantly change during week 30 and week 40 GA ($P > 0.05$). Interestingly, also the level of structural–functional coupling revealed a significant association with age ($r = 0.53$, $P = 0.0137$, Fig. 4*c*), suggesting an increase in coherence between structural and FC of the neonatal brain during prenatal development.

Longitudinal Analysis

Due to the low sample size of longitudinal FC measurements, only an exploratory analysis on possible longitudinal aspects of FC and SC-FC coupling was possible. Longitudinal analysis revealed a positive increase in FC ($P = 0.0467$) and SC-FC coupling ($P = 0.0401$). These findings are consistent with the cross-sectional observations.

Conjectural Implications of White Matter Development on Communication Efficacy Network and Integration Capacity

Communication hubs in the neonatal brain (12 nodes, selected as described above) showed a trend-level increase in betweenness centrality—indicating the level of central placement of hubs in the overall network—over time ($r = 0.28$, $P = 0.15$ ns, Fig. 5*c*), suggestive of a possible, but modest increase in the level of centrality of these nodes in the overall network during development. Figure 5*d* shows this increase in integration capacity between the functional communities between 30 and 40 weeks. With the functional modules describing a modular partitioning of the neonatal brain, the capacity of the underlying structural brain network to integrate information between these subsystems was found to significantly increase over time ($r = 0.45$, $P = 0.0072$).

Longitudinal Analysis

Longitudinal analysis revealed an increase in integration capacity betweeen week 30 and week 40 ($P = 0.0286$, Fig. 6), supporting the notion of a growth of the connectome toward a more global and integrative network over time.

Discussion

Our findings show the early presence of key organizational features of the human connectome, albeit in an immature state and subject to clear developmental changes starting at least as early as in the third trimester of gestation. Collecting and

combining structural and functional neuroimaging data in 27 neonates scanned between week 30 and 40 GA, our study reports on 5 properties of formation and transformation of the early human macroscopic connectome.

First, cortico-cortical white matter pathways of the preterm brain revealed characteristics of a small-world, modular, and hub-including network architecture. Studies have reported on such topological properties of the baby, child, and adult brain, advocating that a small-world modular architecture may be a hallmark feature of macroscopic cortical connectivity (Bassett and Bullmore 2006; Hagmann et al. 2008; Bullmore and Sporns 2009; Fornito et al. 2012; Ratnarajah et al. 2013; Tymofiyeva et al. 2013). Our findings now suggest that these organizational principles are likely to be present from the earliest phases of cortical connectome formation, before term birth. Such an early architecture of the structural connectome is consistent with recent studies showing a small-world organization of the infant functional brain network derived from resting-state fMRI (Fransson et al. 2011) and EEG recordings (Omidvarnia et al. 2014).

Second, overlapping recent reports of the existence of functional hubs in the term neonatal brain based on resting-state fMRI recordings (Fransson et al. 2011), our study shows the existence of a hub structure of the neonatal anatomical connectome. Observed high-degree hub regions overlap the functional hubs as reported by Fransson et al. (2011), classifying (among other regions) the cingulate cortex, superior frontal and superior parietal regions as high-degree hub regions. Interestingly, as mentioned by Fransson et al., the spatial location of these putative hubs tend to show large overlap with both structural and functional hub regions as reported in the adult brain (Hagmann et al. 2008; Gong et al. 2009; van den Heuvel et al. 2010; Zalesky et al. 2010; van den Heuvel and Sporns 2013), suggesting an early presence of connectivity hubs and a neural rich club in the human brain.

Third, our findings suggest an early start of developmental changes in the microstructure of white matter connections. The mean diffusivity and FA values of cortico-cortical tracts displayed clear changes during week 30 and week 40 GA, pointing into the direction of an increase in white matter structure and thus an increase in the efficacy of long-distance neuronal signal transmission in the neonatal brain. These observed developmental changes in white matter microstructure of the neonatal connectome are in clear support of studies reporting global FA and MD changes in the (preterm) neonatal brain (Huppi et al. 1998; Neil et al. 1998; Berman et al. 2005; Bonifacio et al. 2010), as well as with numerous studies showing developmental effects of white matter microstructure during later (>2 years) brain development (e.g., Mukherjee et al. 2002; Schneiderman et al. 2007; Hagmann et al. 2010).

Fourth, outlines of functional communities were observed in the neonatal brain overlapping functional networks as commonly reported for the child and adult brain (e.g., Salvador et al. 2005; Damoiseaux et al. 2006; van den Heuvel et al. 2009; Zuo et al. 2011). No clear developmental changes in these networks could be observed during the examined period here, supporting theories suggesting that most functional networks are present in the early brain, but in an immature state and subject to functional reorganization during later brain development (Dosenbach et al. 2007; Fair et al. 2007, 2009; Fransson et al. 2011).

Fifth, changes in white matter microstructure showed to have a clear impact on the topological structure of the macroscopic structural brain network, revealing an increase in small-world network characteristics. Such a developmental gradient is supported by the results of the performed computational modeling analysis, showing an increase in the network's integration capacity between week 30 and week 40 GA. These findings suggest that connectome development is accompanied by an increase of the brain system to consolidate information from different functional subnetworks, which is in support of modern theories hypothesizing that development of the child and adolescent brain involves an increasing capacity of the network to integrate information between its subparts (Dosenbach et al. 2007; Fair et al. 2008).

Within the infant and child brain, white matter development has been suggested to mostly involve ongoing myelination of axonal projections, a developmental process that is suggested to continue at least throughout adolescence (e.g., Hagmann et al. 2008; Peper et al. 2009). Postmortem myelogenetic maps have shown myelination of primordial regions at birth, while myelination of tertiary association regions and their tracts suggested to start after birth (see for review, Catani et al. (2013)). Animal studies of white matter development have indeed suggested that large-scale myelination processes of cortico-cortical association tracts do not start before the onset of (term) birth (LaMantia and Rakic 1990, 1994), with prenatal white matter development predominantly involving an increase in total number of axons and an increase in the variation of axonal diameter of axons in white matter pathways (LaMantia and Rakic 1990). Our neuroimaging observations of increasing FA and decreasing MD/TD signal between week 30 and week 40 GA may thus also reflect, to some extent, developmental changes in the diameter of axons and an ongoing growth in axonal count of the examined cortico-cortical pathways (Nossin-Manor et al. 2012). To the best of our knowledge, no previous reports have been made on in vivo changes in axonal count or axonal diameter of macroscopic white matter bundles in the immature human brain on basis of neuroimaging observations. A clear delineation of the different processes of microstructural white matter development is out of range of current imaging techniques, but new advances in neuroimaging might provide more detailed measurements of axonal microstructure in the near future (Johansen-Berg and Rushworth 2009; Alexander et al. 2010; Jbabdi and Johansen-Berg 2011), allowing further understanding of the underlying processes of formation, growth, and transformation of macroscopic brain connectivity during this crucial period of brain development.

The early presence of a small-world and rich club topology may suggest the existence of an underlying "connectivity blueprint" of the human brain. High consistency of connectivity patterns across mammalian species (Markov et al. 2011; Goulas et al. 2014; Harriger et al. 2012; Shi et al. 2012; de Reus and Van den Heuvel 2013), together with findings of a genetic background of brain networks (Glahn et al. 2010; Fornito et al. 2011; van den Heuvel et al. 2012) indeed suggest the existence of a somewhat predefined, likely genetically driven, layout of macroscopic connectivity of the human brain. Our findings do not, however, necessarily imply that the trajectories of white matter pathways are completely predetermined. Tract tracing data of the developing kitten brain have revealed spatially widespread termination zones of long-range visual corpus callosum tracts in kittens at post-term day 4, followed by a relative short period (days to weeks) in which spatial specialization of tracts and their termination zones occurs (see for review, Innocenti and Price (2005)). Such a, potential nonspecific,

overgrowth of macroscopic connectivity is further supported by observations of corpus callosal and associative tracts in young rhesus monkeys, revealing the highest number of axonal connections at birth, followed by a 70% decrease in axonal count in the first postnatal weeks (Price and Ferrer 1993; LaMantia and Rakic 1994). Thus, despite the presence of a putative small-world type architecture of the human brain at term birth, one might speculate about the notion of a, to some extent, initially random-shaped layout of cortico-cortical connections at connectome genesis, with rapid pruning and specialization of white matter connections after birth (LaMantia and Rakic 1990; Price and Ferrer 1993; Innocenti and Price 2005).

Our results are inherently limited by both the nature of the noninvasive imaging techniques involves, as well as by the group of participants. First, as mentioned, the majority of connections in the human brain involve intracortical and very short intracortical axonal projections (Schuz and Braitenberg 2002; Markov et al. 2011), connections that are well out of reach for current day neuroimaging diffusion and resting-state fMRI technology that operate at the millimeter to centimeter resolution. In contrast, only a fraction of all neural interactions involve long-range associative and commissural white matter projections and form the "macroscale connectome" (Sporns 2011, 2012). It is this class of connections that is, at the macroscale, within the reach of modern neuroimaging techniques, as also used in this study. However, in this context, it is important to note that noninvase neuroimaging techniques only provide "reconstructions" of large bundles of neural connections, and do not directly measure or asses individual neural projections. As a result, both diffusion imaging and functional MRI techniques suffer from many limitations, like the complex reconstruction of projections where the diffusion signal is not uniform as in points were multiple fiber bundles cross or pass (e.g., Jones 2008; Johansen-Berg and Rushworth 2009; Jbabdi and Johansen-Berg 2011), the inclusion of false-positive and false-negative connection reconstructions (e.g., de Reus and van den Heuvel 2012) and a known influence of postprocessing steps on the reconstructions and subsequent graph analytical analysis of the data (e.g., Zalesky et al. 2010; Fornito et al. 2012; Power et al. 2012; de Reus and van den Heuvel 2013). Despite these limitations, at the macroscale, studies have shown consistent results of key features of connectome organization across different acquisition and analysis techniques, as well across different species (e.g., Bassett et al. 2009; Markov et al. 2013; Park and Friston 2013; van den Heuvel and Sporns 2013; de Lange et al. 2014). Together, these findings suggest that diffusion imaging and functional MRI are useful approaches to map and examine the topological organization of human connectome at the macroscale (Bullmore and Sporns 2009; van den Heuvel and Hulshoff Pol 2010; Sporns 2012; Jbabdi and Behrens 2013) and study the interaction between anatomical connectivity and functional brain dynamics (Hagmann et al. 2008; Honey and Sporns 2008; Collin et al. 2014; van den Heuvel and Sporns 2013; Senden et al. 2014). Furthermore, it provides a promising platform to examine the genetic contribution to the formation of macroscale brain connectivity (Fornito et al. 2011; van den Heuvel et al. 2012; Jahanshad et al. 2013), examine structural and functional dysconnectivity effects in neurological and psychiatric disorders (e.g., Bassett and Bullmore 2009; Buckner et al. 2009; Fornito et al. 2012; Filippi et al. 2013), and in particular study how disrupted and/or deviating development of brain connectivity may relate to the development of brain disorders (e.g., Dosenbach et al. 2010; Boersma et al. 2013; Dennis and Thompson 2013; van den Heuvel and Fornito 2014).

Second, concerning the nature of the included population, all of our data were acquired post birth, with neonatal development continuing in an incubator environment. Third, as most studies concerning neonatal development, also our study contains a relative small group of subjects when compared with imaging studies performed in older children and adults. This is particular the case for our developmental longitudinal analysis, which included only a small subset of inclusions, and the results of this analysis should therefore be interpreted as exploratory and preliminary. Fourth, the acquisition of neonatal data is a specialized task, and similar to most neonatal studies, scans were acquired as part of standard clinical care. As a result, the included group is rather heterogenous (birth weight varied between 460 and 1360 g, with 19 neonates showing mild brain injury as shown on a conventional image, see Table 1). Furthermore, preterm born neonates often have brain lesions, developed in the perinatal period, which may lead to a deviating pattern of brain development (Pandit et al. 2014) and affected cognitive functioning later in life (Mulder et al. 2009; Aarnoudse-Moens et al. 2013). To reflect the processes of normal development as much as possible, only neonates without major morbidity on their conventional MR-imaging were included in our study. Fifth, scan-time is limited in a clinical setting, and as a result the diffusion imaging sequence involved a relative low number of directions (32 directions), when compared with adult studies. And sixth, all data were acquired under sedation which may influence the acquisition of the resting-state fMRI data (e.g., Liu et al. 2013). Nevertheless, neonatal FC patterns showed relative high overlap with patterns as observed in non-sedated, awake adults. Others have indeed reported that sedation during scanning does not have a strong influence on global FC patterns and the formation of resting-state networks (Fransson et al. 2007).

This report demonstrates the presence of an early small-world modular architecture of the human neonatal connectome. Our findings suggest that a development toward a more efficient and more integrative brain network forms one of the key biological algorithms that shape macroscopic connectivity in the early human connectome.

Supplementary Material

Supplementary material can be found at: http://www.cercor.oxfordjournals.org/

Funding

MPvdH is supported by a Fellowship of the Brain Center Rudolf Magnus and a VENI grant of the Dutch Council for Research (VENI: 451-12-001 NWO). Funding to pay the Open Access publication charges for this article was provided by the Dutch Research Council (NWO).

Notes

Conflict of Interest: None declared.

References

Aarnoudse-Moens CS, Weisglas-Kuperus N, Duivenvoorden HJ, van Goudoever JB, Oosterlaan J. 2013. Executive function and IQ predict mathematical and attention problems in very preterm children. PLoS One. 8:e55994.

Adams E, Chau V, Poskitt KJ, Grunau RE, Synnes A, Miller SP. 2010. Tractography-based quantitation of corticospinal tract development in premature newborns. J Pediatr. 156:882–888. 888 e881.

Alexander DC, Hubbard PL, Hall MG, Moore EA, Ptito M, Parker GJ, Dyrby TB. 2010. Orientationally invariant indices of axon diameter and density from diffusion MRI. Neuroimage. 52:1374–1389.

Andersson JL, Skare S. 2002. A model-based method for retrospective correction of geometric distortions in diffusion-weighted EPI. Neuroimage. 16:177–199.

Bassett DS, Brown JA, Deshpande V, Carlson JM, Grafton ST. 2010. Conserved and variable architecture of human white matter connectivity. Neuroimage. 54:1262–1279.

Bassett DS, Bullmore ET. 2009. Human brain networks in health and disease. Curr Opin Neurol. 22:340–347.

Bassett DS, Bullmore E. 2006. Small-world brain networks. Neuroscientist. 12:512–523.

Bassett DS, Bullmore ET, Meyer-Lindenberg A, Apud JA, Weinberger DR, Coppola R. 2009. Cognitive fitness of cost-efficient brain functional networks. Proc Natl Acad Sci USA. 106:11747–11752.

Beaulieu C, Allen PS. 1994. Water diffusion in the giant axon of the squid: implications for diffusion-weighted MRI of the nervous system. Magn Reson Med. 32:579–583.

Berman JI, Mukherjee P, Partridge SC, Miller SP, Ferriero DM, Barkovich AJ, Vigneron DB, Henry RG. 2005. Quantitative diffusion tensor MRI fiber tractography of sensorimotor white matter development in premature infants. Neuroimage. 27:862–871.

Boersma M, Kemner C, De Reus M, Collin G, Snijders T, Hofman D, Buitelaar J, Stam C, van den Heuvel M. 2013. Disrupted functional brain networks in autistic toddlers. Brain Connect. 3(1):41–49.

Bonifacio SL, Glass HC, Chau V, Berman JI, Xu D, Brant R, Barkovich AJ, Poskitt KJ, Miller SP, Ferriero DM. 2010. Extreme premature birth is not associated with impaired development of brain microstructure. J Pediatr. 157:726–732. e721.

Bruer J. 1999. Neural connections: some you use, some you lose. In: The myth of the first three years. Chapter 3. Simon & Schuster, Free Press.

Buckner RL, Sepulcre J, Talukdar T, Krienen FM, Liu H, Hedden T, Andrews-Hanna JR, Sperling RA, Johnson KA. 2009. Cortical hubs revealed by intrinsic functional connectivity: mapping, assessment of stability, and relation to Alzheimer's disease. J Neurosci. 29:1860–1873.

Bullmore E, Sporns O. 2009. Complex brain networks: graph theoretical analysis of structural and functional systems. Nat Rev Neurosci. 10:186–198.

Bystron I, Blakemore C, Rakic P. 2008. Development of the human cerebral cortex: Boulder Committee revisited. Nat Rev Neurosci. 9:110–122.

Catani M, Thiebaut de Schotten M, Slater D, Dell'acqua F. 2013. Connectomic approaches before the connectome. Neuroimage. 80:2–13.

Chang LC, Jones DK, Pierpaoli C. 2005. RESTORE: robust estimation of tensors by outlier rejection. Magn Reson Med. 53:1088–1095.

Colizza V, Flammini A, Serrano MA, Vespignani A. 2006. Detecting rich-club ordering in complex networks. Nat Phys. 2:110–115.

Collin G, Sporns O, Mandl RC, van den Heuvel MP. 2014. Structural and functional aspects relating to cost and benefit of rich club organization in the human cerebral cortex. Cereb Cortex. 24: 2258–2267.

Collin G, van den Heuvel MP. 2013. The ontogeny of the human connectome: development and dynamic changes of brain connectivity across the life span. Neuroscientist. 19:616–628.

Damoiseaux JS, Rombouts SA, Barkhof F, Scheltens P, Stam CJ, Smith SM, Beckmann CF. 2006. Consistent resting-state networks across healthy subjects. Proc Natl Acad Sci USA. 103:13848–13853.

Deipolyi AR, Mukherjee P, Gill K, Henry RG, Partridge SC, Veeraraghavan S, Jin H, Lu Y, Miller SP, Ferriero DM et al. 2005. Comparing microstructural and macrostructural development of the cerebral cortex in premature newborns: diffusion tensor imaging versus cortical gyration. Neuroimage. 27:579–586.

de Lange SC, de Reus MA, van den Heuvel MP. 2014. The Laplacian spectrum of neural networks. Front Comput Neurosci. 7:189.

Dennis EL, Thompson PM. 2013. Typical and atypical brain development: a review of neuroimaging studies. Dialogues Clin Neurosci. 15:359–384.

de Reus MA, van den Heuvel MP. 2012. Estimating false positives and negatives in brain networks. Neuroimage. 70:402–409.

de Reus MA, van den Heuvel MP. 2013. The parcellation-based connectome: limitations and extensions. Neuroimage. 80:397–404.

Dosenbach NU, Fair DA, Miezin FM, Cohen AL, Wenger KK, Dosenbach RA, Fox MD, Snyder AZ, Vincent JL, Raichle ME et al. 2007. Distinct brain networks for adaptive and stable task control in humans. Proc Natl Acad Sci USA. 104:11073–11078.

Dosenbach NU, Nardos B, Cohen AL, Fair DA, Power JD, Church JA, Nelson SM, Wig GS, Vogel AC, Lessov-Schlaggar CN et al. 2010. Prediction of individual brain maturity using fMRI. Science. 329: 1358–1361.

Eguiluz VM, Chialvo DR, Cecchi GA, Baliki M, Apkarian AV. 2005. Scale-free brain functional networks. Phys Rev Lett. 94:018102.

Fair DA, Cohen AL, Dosenbach NU, Church JA, Miezin FM, Barch DM, Raichle ME, Petersen SE, Schlaggar BL. 2008. The maturing architecture of the brain's default network. Proc Natl Acad Sci USA. 105:4028–4032.

Fair DA, Cohen AL, Power JD, Dosenbach NU, Church JA, Miezin FM, Schlaggar BL, Petersen SE. 2009. Functional brain networks develop from a "local to distributed" organization. PLoS Comput Biol. 5:e1000381.

Fair DA, Dosenbach NU, Church JA, Cohen AL, Brahmbhatt S, Miezin FM, Barch DM, Raichle ME, Petersen SE, Schlaggar BL. 2007. Development of distinct control networks through segregation and integration. Proc Natl Acad Sci USA. 104:13507–13512.

Filippi M, van den Heuvel MP, Fornito A, He Y, Hulshoff Pol HE, Agosta F, Comi G, Rocca MA. 2013. Assessment of system dysfunction in the brain through MRI-based connectomics. Lancet Neurol. 12:1189–1199.

Fornito A, Zalesky A, Bassett DS, Meunier D, Ellison-Wright I, Yucel M, Wood SJ, Shaw K, O'Connor J, Nertney D et al. 2011. Genetic influences on cost-efficient organization of human cortical functional networks. J Neurosci. 31:3261–3270.

Fornito A, Zalesky A, Pantelis C, Bullmore ET. 2012. Schizophrenia, neuroimaging and connectomics. Neuroimage. 12(12):1189–1199.

Fransson P, Aden U, Blennow M, Lagercrantz H. 2011. The functional architecture of the infant brain as revealed by resting-state fMRI. Cereb Cortex. 21:145–154.

Fransson P, Skiold B, Engstrom M, Hallberg B, Mosskin M, Aden U, Lagercrantz H, Blennow M. 2009. Spontaneous brain activity in the newborn brain during natural sleep—an fMRI study in infants born at full term. Pediatr Res. 66:301–305.

Fransson P, Skiold B, Horsch S, Nordell A, Blennow M, Lagercrantz H, Aden U. 2007. Resting-state networks in the infant brain. Proc Natl Acad Sci USA. 104:15531–15536.

Glahn DC, Winkler AM, Kochunov P, Almasy L, Duggirala R, Carless MA, Curran JC, Olvera RL, Laird AR, Smith SM et al. 2010. Genetic control over the resting brain. Proc Natl Acad Sci USA. 107: 1223–1228.

Gong G, He Y, Concha L, Lebel C, Gross DW, Evans AC, Beaulieu C. 2009. Mapping anatomical connectivity patterns of human cerebral cortex using in vivo diffusion tensor imaging tractography. Cereb Cortex. 19:524–536.

Goulas A, Uylings HB, Stiers P. 2014. Mapping the hierarchical layout of the structural network of the macaque prefrontal cortex. Cereb Cortex. 24:1178–1194 .

Hagmann P, Cammoun L, Gigandet X, Meuli R, Honey CJ, Wedeen VJ, Sporns O. 2008. Mapping the structural core of human cerebral cortex. PLoS Biol. 6:e159.

Hagmann P, Sporns O, Madan N, Cammoun L, Pienaar R, Wedeen VJ, Meuli R, Thiran JP, Grant PE. 2010. White matter maturation reshapes structural connectivity in the late developing human brain. Proc Natl Acad Sci USA. 107:19067–19072.

Harriger L, van den Heuvel MP, Sporns O. 2012. Rich club organization of macaque cerebral cortex and its role in network communication. PLoS One. 7:e46497.

Honey CJ, Sporns O. 2008. Dynamical consequences of lesions in cortical networks. Hum Brain Mapp. 29:802–809.
Honey CJ, Sporns O, Cammoun L, Gigandet X, Thiran JP, Meuli R, Hagmann P. 2009. Predicting human resting-state functional connectivity from structural connectivity. Proc Natl Acad Sci USA. 106:2035–2040.
Humphries MD, Gurney K, Prescott TJ. 2006. The brainstem reticular formation is a small-world, not scale-free, network. Proc Biol Sci. 273:503–511.
Huppi PS, Maier SE, Peled S, Zientara GP, Barnes PD, Jolesz FA, Volpe JJ. 1998. Microstructural development of human newborn cerebral white matter assessed in vivo by diffusion tensor magnetic resonance imaging. Pediatr Res. 44:584–590.
Huttenlocher PR, Dabholkar AS. 1997. Regional differences in synaptogenesis in human cerebral cortex. J Comp Neurol. 387:167–178.
Hwang K, Hallquist MN, Luna B. 2012. The development of hub architecture in the human functional brain network. Cereb Cortex. 23:2380–2393.
Innocenti GM, Price DJ. 2005. Exuberance in the development of cortical networks. Nat Rev Neurosci. 6:955–965.
Jahanshad N, Rajagopalan P, Hua X, Hibar DP, Nir TM, Toga AW, Jack CR Jr, Saykin AJ, Green RC, Weiner MW et al. 2013. Genome-wide scan of healthy human connectome discovers SPON1 gene variant influencing dementia severity. Proc Natl Acad Sci USA. 110:4768–4773.
Jbabdi S, Behrens TE. 2013. Long-range connectomics. Ann N Y Acad Sci. 1305:83–93.
Jbabdi S, Johansen-Berg H. 2011. Tractography: where do we go from here? Brain Connect. 1:169–183.
Johansen-Berg H, Rushworth MF. 2009. Using diffusion imaging to study human connectional anatomy. Annu Rev Neurosci. 32:75–94.
Jones DK. 2008. Studying connections in the living human brain with diffusion MRI. Cortex. 44:936–952.
Khundrakpam BS, Reid A, Brauer J, Carbonell F, Lewis J, Ameis S, Karama S, Lee J, Chen Z, Das S et al. 2012. Developmental changes in organization of structural brain networks. Cereb Cortex. 23:2072–2085.
Kostovic I, Jovanov-Milosevic N, Rados M, Sedmak G, Benjak V, Kostovic-Srzentic M, Vasung L, Culjat M, Rados M, Huppi P et al. 2014. Perinatal and early postnatal reorganization of the subplate and related cellular compartments in the human cerebral wall as revealed by histological and MRI approaches. Brain Struct Funct. 219:231–253.
Lagercrantz HE. 1998. The newborn brain: neuroscience and clinical applications. Cambridge: Cambridge University Press.
LaMantia AS, Rakic P. 1994. Axon overproduction and elimination in the anterior commissure of the developing rhesus monkey. J Comp Neurol. 340:328–336.
LaMantia AS, Rakic P. 1990. Axon overproduction and elimination in the corpus callosum of the developing rhesus monkey. J Neurosci. 10:2156–2175.
Liu X, Pillay S, Li R, Vizuete JA, Pechman KR, Schmainda KM, Hudetz AG. 2013. Multiphasic modification of intrinsic functional connectivity of the rat brain during increasing levels of propofol. Neuroimage. 83:581–592.
Mantel N. 1967. The detection of disease clustering and a generalized regression approach. Cancer Res. 27:209–220.
Markov NT, Ercsey-Ravasz M, Van Essen DC, Knoblauch K, Toroczkai Z, Kennedy H. 2013. Cortical high-density counterstream architectures. Science. 342:1238406.
Markov NT, Misery P, Falchier A, Lamy C, Vezoli J, Quilodran R, Gariel MA, Giroud P, Ercsey-Ravasz M, Pilaz LJ et al. 2011. Weight consistency specifies regularities of macaque cortical networks. Cereb Cortex. 21:1254–1272.
Maslov S, Sneppen K. 2002. Specificity and stability in topology of protein networks. Science. 296:910–913.
Molliver ME, Kostović I, Van der Loos H. 1973. The development of synapses in cerebral cortex of the human fetus. Brain Res. 50:403–407.
Mori S, van Zijl PC. 2002. Fiber tracking: principles and strategies—a technical review. NMR Biomed. 15:468–480.
Mukherjee P, Miller JH, Shimony JS, Philip JV, Nehra D, Snyder AZ, Conturo TE, Neil JJ, McKinstry RC. 2002. Diffusion-tensor MR imaging of gray and white matter development during normal human brain maturation. AJNR Am J Neuroradiol. 23:1445–1456.
Mulder H, Pitchford NJ, Hagger MS, Marlow N. 2009. Development of executive function and attention in preterm children: a systematic review. Dev Neuropsychol. 34:393–421.
Neil JJ, Shiran SI, McKinstry RC, Schefft GL, Snyder AZ, Almli CR, Akbudak E, Aronovitz JA, Miller JP, Lee BC et al. 1998. Normal brain in human newborns: apparent diffusion coefficient and diffusion anisotropy measured by using diffusion tensor MR imaging. Radiology. 209:57–66.
Newman ME. 2006. Modularity and community structure in networks. Proc Natl Acad Sci USA. 103:8577–8582.
Nossin-Manor R, Card D, Morris D, Noormohamed S, Shroff MM, Whyte HE, Taylor MJ, Sled JG. 2012. Quantitative MRI in the very preterm brain: assessing tissue organization and myelination using magnetization transfer, diffusion tensor and T(1) imaging. Neuroimage. 64:505–516.
Oishi K, Mori S, Donohue PK, Ernst T, Anderson L, Buchthal S, Faria A, Jiang H, Li X, Miller MI et al. 2011. Multi-contrast human neonatal brain atlas: application to normal neonate development analysis. Neuroimage. 56:8–20.
Omidvarnia A, Fransson P, Metsaranta M, Vanhatalo S. 2014. Functional bimodality in the brain networks of preterm and term human newborns. Cereb Cortex. 24:2657–2668.
Pandit AS, Robinson E, Aljabar P, Ball G, Gousias IS, Wang Z, Hajnal JV, Rueckert D, Counsell SJ, Montana G et al. 2014. Whole-brain mapping of structural connectivity in infants reveals altered connection strength associated with growth and preterm birth. Cereb Cortex. 24:2324–2333.
Papile LA, Burstein J, Burstein R, Koffler H. 1978. Incidence and evolution of supependymal and intraventricular hemorrhage:a study of infants with birth weights less than 1500 gm. J Pediatrics. 92:529–534.
Park HJ, Friston K. 2013. Structural and functional brain networks: from connections to cognition. Science. 342:1238411.
Peper JS, Schnack HG, Brouwer RM, Van Baal GC, Pjetri E, Szekely E, van Leeuwen M, van den Berg SM, Collins DL, Evans AC et al. 2009. Heritability of regional and global brain structure at the onset of puberty: a magnetic resonance imaging study in 9-year-old twin pairs. Hum Brain Mapp. 30:2184–2196.
Petanjek Z, Judas M, Simic G, Rasin MR, Uylings HB, Rakic P, Kostovic I. 2011. Extraordinary neoteny of synaptic spines in the human prefrontal cortex. Proc Natl Acad Sci USA. 108:13281–13286.
Power JD, Barnes KA, Snyder AZ, Schlaggar BL, Petersen SE. 2012. Spurious but systematic correlations in functional connectivity MRI networks arise from subject motion. Neuroimage. 59:2142–2154.
Power JD, Fair DA, Schlaggar BL, Petersen SE. 2010. The development of human functional brain networks. Neuron. 67:735–748.
Price DJ, Ferrer JM. 1993. The incidence of bifurcation among corticocortical connections from area 17 in the developing visual cortex of the cat. Eur J Neurosci. 5:223–231.
Rakic P, Bourgeois JP, Eckenhoff MF, Zecevic N, Goldman-Rakic PS. 1986. Concurrent overproduction of synapses in diverse regions of the primate cerebral cortex. Science. 232:232–235.
Ratnarajah N, Rifkin-Graboi A, Fortier MV, Chong YS, Kwek K, Saw SM, Godfrey KM, Gluckman PD, Meaney MJ, Qiu A. 2013. Structural connectivity asymmetry in the neonatal brain. Neuroimage. 75:195–202.
Rubinov M, Sporns O. 2010. Complex network measures of brain connectivity: uses and interpretations. Neuroimage. 52:1059–1069.
Rubinov M, Sporns O. 2011. Weight-conserving characterization of complex functional brain networks. Neuroimage. 56:2068–2079.
Salvador R, Suckling J, Coleman MR, Pickard JD, Menon D, Bullmore E. 2005. Neurophysiological architecture of functional magnetic resonance images of human brain. Cereb Cortex. 15:1332–1342.
Satterthwaite TD, Wolf DH, Loughead J, Ruparel K, Elliott MA, Hakonarson H, Gur RC, Gur RE. 2013. Impact of in-scanner head motion on multiple measures of functional connectivity: relevance

for studies of neurodevelopment in youth. Neuroimage. 60: 623–632.
Schneiderman JS, Buchsbaum MS, Haznedar MM, Hazlett EA, Brickman AM, Shihabuddin L, Brand JG, Torosjan Y, Newmark RE, Tang C et al. 2007. Diffusion tensor anisotropy in adolescents and adults. Neuropsychobiology. 55:96–111.
Schuz A, Braitenberg V. 2002. The human cortial white matter: quantitative aspects of cortico-cortical long-range connectivity. In: Schuz A, Miller R, editors. Cortical Areas: Unity and Diversity.
Senden M, Deco G, Goebel R, van den Heuvel MP. 2014. Rich club organization supports a diverse set of functional network configurations. Neuroimage. 96:174–182.
Shi F, Yap PT, Gao W, Lin W, Gilmore JH, Shen D. 2012. Altered structural connectivity in neonates at genetic risk for schizophrenia: a combined study using morphological and white matter networks. Neuroimage. 62:1622–1633.
Smyser CD, Snyder AZ, Neil JJ. 2011. Functional connectivity MRI in infants: exploration of the functional organization of the developing brain. Neuroimage. 56:1437–1452.
Sporns O. 2012. Discovering the human connectome. Cambridge: MIT Press.
Sporns O. 2011. The human connectome: a complex network. Ann N Y Acad Sci. 1224:109–125.
Sporns O, Tononi G, Kotter R. 2005. The human connectome: a structural description of the human brain. PLoS Comput Biol. 1: e42.
Stevens MC, Pearlson GD, Calhoun VD. 2009. Changes in the interaction of resting-state neural networks from adolescence to adulthood. Hum Brain Mapp. 30:2356–2366.
Stiles J, Jernigan TL. 2010. The basics of brain development. Neuropsychol Rev. 20:327–348.
Tymofiyeva O, Hess CP, Ziv E, Tian N, Bonifacio SL, McQuillen PS, Ferriero DM, Barkovich AJ, Xu D. 2013. Towards the "baby connectome": mapping the structural connectivity of the newborn brain. PLoS One. 7:e31029.
van den Heuvel MP, Fornito A. 2014. Brain networks in schizophrenia. Neuropsychol Rev. 24:32–48.
van den Heuvel MP, Hulshoff Pol HE. 2010. Exploring the brain network: a review on resting-state fMRI functional connectivity. Eur Neuropsychopharmacol. 20:519–534.
van den Heuvel MP, Mandl RCW, Kahn RS, Hulshoff Pol HE. 2009. Functionally linked resting state networks reflect the underlying structural connectivity architecture of the human brain. Hum Brain Mapp. 30:3127–3141.
van den Heuvel MP, Mandl RCW, Stam CJ, Kahn RS, Hulshoff Pol HE. 2010. Aberrant frontal and temporal network structure in schizophrenia: a graph theoretical analysis. J Neurosci. 30: 15915–15926.
van den Heuvel MP, Sporns O. 2013. An anatomical substrate for integration among functional networks in human cortex. J Neurosci. 33:14489–14500.
van den Heuvel MP, Sporns O. 2013. Network hubs of the human brain. Trends Cogn Sci. 17(12):683–696.
van den Heuvel MP, Sporns O. 2011. Rich-club organization of the human connectome. J Neurosci. 31:15775–15786.
van den Heuvel MP, Sporns O, Collin G, Scheewe T, Mandl RC, Cahn W, Goni J, Hulshoff Pol HE, Kahn RS. 2013. Abnormal rich club organization and functional brain dynamics in schizophrenia. JAMA Psychiatry. 70:783–792.
van den Heuvel MP, Stam CJ, Boersma M, Hulshoff Pol HE. 2008. Small-world and scale-free organization of voxel based resting-state functional connectivity in the human brain. Neuroimage. 43:528–539.
van den Heuvel MP, van Soelen IL, Stam CJ, Kahn RS, Boomsma DI, Hulshoff Pol HE. 2012. Genetic control of functional brain network efficiency in children. Eur Neuropsychopharmacol. 23:19–23.
Van Dijk KR, Sabuncu MR, Buckner RL. 2011. The influence of head motion on intrinsic functional connectivity MRI. Neuroimage. 59: 431–438.
Woodward LJ, Anderson PJ, Austin NC, Howard K, Inder TE. 2006. Neonatal MRI to predict neurodevelopmental outcomes in preterm infants. N Engl J Med. 355:685–694.
Yap PT, Fan Y, Chen Y, Gilmore JH, Lin W, Shen D. 2011. Development trends of white matter connectivity in the first years of life. PLoS One. 6:e24678.
Zalesky A, Fornito A, Harding IH, Cocchi L, Yucel M, Pantelis C, Bullmore ET. 2010. Whole-brain anatomical networks: does the choice of nodes matter? Neuroimage. 50:970–983.
Zamora-Lopez G, Zhou C, Kurths J. 2010. Cortical hubs form a module for multisensory integration on top of the hierarchy of cortical networks. Front Neuroinform. 4:1. doi: 10.3389.
Zuo XN, Ehmke R, Mennes M, Imperati D, Castellanos FX, Sporns O, Milham MP. 2011. Network centrality in the human functional connectome. Cereb Cortex. 22:1862–1875.